Numerical simulation of urea based selective non-catalytic reduction deNOx process for industrial applications

Jakov Baleta*, Hrvoje Mikulčić, Milan Vujanović, Zvonimir Petranović, Neven Duić

Faculty of Mechanical Engineering and Naval Architecture

University of Zagreb, Zagreb, Croatia

e–mail: jakov.baleta@fsb.hr

ABSTRACT

Industrial processes emit large amounts of diverse pollutants into the atmosphere, among which NOx takes a significant portion. Selective non-catalytic reduction (SNCR) is a relatively simple method for the NOx reduction in large industrial facilities such as power plants, cement plants and waste incinerator plants. It consists of injecting the urea-water solution in the hot flue gas stream and its reaction with the NOx. During this process flue gas enthalpy is used for the urea-water droplet heating and for the evaporation of water content. After water evaporates, thermolysis of urea occurs, during which ammonia, a known NO_x reductant, and isocyanic acid are generated. In order to cope with the ever stringent environmental norms, equipment manufacturers need to develop energy efficient products that are at the same time benign to environment. This is becoming increasingly complicated and costly, and one way to reduce production costs together with the maintaining the same competitiveness level is to employ computational fluid dynamics (CFD) as a tool, in a process today commonly known under the term "virtual prototyping".

* Corresponding author

The aim of this paper is to show capabilities of the developed mathematical framework implemented in the commercial CFD code AVL FIRE®, to simulate physical processes of all relevant phenomena occurring during the SNCR process. First, mathematical models for description of SNCR process are presented and afterwards, models are used on the 3D geometry of an industrial reactor and a real industrial case to predict SNCR efficiency, temperature and velocity field. Influence of the main operational parameters on NOx reduction efficiency was performed on the same case. Finally, conclusions about validity of current framework are given together with recommendations for further work.

Key words: computational fluid dynamics, NOx reduction, selective non-catalytic reduction, reaction kinetics, urea-water solution, Lagrangian spray

1. INTRODUCTION

The latest report from the scientific panel on anthropogenic global warming indicates that remarkable and joint global action is required to reduce greenhouse gas emission and harmful emissions in generally, and the longer we wait to address this issue, the more difficult, technologically challenging and expensive it will become [1].

Fossil fuel burning in industry, fertilisers containing nitrogen and transport produce the majority of NO_x emissions. Nitrogen-oxides (NO_x) contribute to acid deposition and eutrophication of soil and water. The subsequent impacts of acid deposition can be significant, including adverse effects on aquatic ecosystems in rivers and lakes and damage to forests, crops and other vegetation. Eutrophication can lead to severe reductions in water quality with subsequent impacts including decreased biodiversity, changes in species composition and dominance, and toxicity effects. NO_2 is associated with adverse effects on human health and also contributes to the formation of secondary particulate aerosols and tropospheric ozone in the atmosphere, both of which are important air pollutants due to their adverse impacts on human health and other climate effects [2].

Despite the fact that the European Environment Agency (EEA)-33 emissions of nitrogen oxides (NOx) decreased by 44% between 1990 and 2011 [2], they are still subject to the current and upcoming emission standards [3] in order to minimize their harmful environmental impact. In 2011, the most significant sources of NOx emissions were road transport (41%), energy production and distribution (23%) and the commercial, institutional and households (13%) sectors [2].

Amount of formed NOx is influenced by several factors such as combustion temperature, flow velocity field in combustion chamber, design of the combustion chamber and burner, fuel composition, ratio of fuel and air dosage, etc. There are three kinds of NOx production mechanisms taking place during combustion processes: fuel NOx, thermal NOx and prompt NOx [4]. Fuel NOx is produced from the oxidation of fuel bonded nitrogen, whilst thermal and prompt NOx require atmospheric nitrogen for reaction. Production of the fuel NOx is especially pronounced in the cases of coal and biomass combustion due to the relatively high content of fuel contained nitrogen [5]. Triple bonds in the nitrogen molecules could be broken only by introducing large amount of energy in the reaction system. Therefore, thermal NOx is only formed in significant quantities at temperatures above 1500°C.

Methods of NOx control may be categorized into primary methods, which prevent formation of NOx and secondary NOx control methods, which are focused on the reduction of already formed NOx [6]. Selection of individual method or combination of methods is always conditioned by economic balances and legislation.

First option of primary NOx control methods consists of regulation of the excess air, keeping at the same time in mind the fact that it directly affects unburned carbon emissions. Combustion air staging creates fuel-rich primary zone and fuel-lean secondary zone, supressing that way creation of fuel and thermal NOx. Similarly like combustion air, fuel can also be staggered through creating a fuel-rich secondary combustion zone, where NOx formed in the primary combustion

zone is decomposed. Exhaust gas recirculation, a technique frequently employed in modern internal combustion engines [7], as well represents one of the primary NOx reduction measures which can significantly reduce thermal NOx generation by lowering combustion temperatures and excess air. Tightened NOx emission standards [8,9] on industrial emissions from combustion plants cannot be met using described primary NOx reduction techniques anymore. Also, it is difficult to implement those techniques into existing facilities. Taking stated into account, it can be clearly seen that the answer to those challenges should be found in utilizing exhaust gas aftertreatment. Although some new technologies emerged during the last few years, such as pulsed corona discharge and electron beam flue gas treatment [4], selective non-catalytic reduction (SNCR) as well as selective catalytic reduction (SCR) have proven to be optimal from both the cost and NOx reduction efficiency view point.

SCR offers higher denitrification efficiencies with respect to SNCR, although investment cost is much higher [10] and it is not suitable for retrofitting due to clogging problems and loose of catalytic efficiency in such cases. On the other side, SNCR is a proven cost-effective secondary method of NOx control from big stationary sources such as power plants, incinerators, boilers and cement calciners. The process is operated by the controlled injection of reducing agents such as ammonia or urea [11]. The performance of SNCR process has been shown to be influenced by reducing agent residence time, temperature profile in reaction zone, quality of mixing of reagent with flue gases, concentration of NOx in flue gases, ammonia slip and normalized stoichiometric ratio [12]. Residence time is a factor whose increase enables longer contact between reducing agent and NOx. Its value is highly dependent on flow geometry and velocities inside the region where SNCR is taking place. Most researchers agree that optimum SNCR process is taking place within relatively narrow temperature range between 800 and 1100°C [10]. Above this temperature ammonia tends to oxidize and below the 800°C reduction rate is too slow. Mixing quality of reagent and exhaust gases is dependent upon velocities and swirl in reaction zone, and

also upon the injecting conditions, whilst the concentration of NOx in flue gases could be affected using primary NOx reduction measurements, and also differs between various applications such as power plants, utility boilers, incinerators, etc. Normalized stoichiometric ratio (NSR) refers to the ratio between reducing agent and NOx. It is preferable to have it high but one must take into account also toxic ammonia slip which is limited by various legislations and norms. Previous research showed that optimum NSR value in terms of NO reduction efficiency is between 1.5 and 2 [13].

All operating conditions are interdependent and show that, although SNCR process is principally very simple, design of optimum process or retrofitting existing facility is far beyond trivial. There are several arguments for using computational fluid dynamics in SNCR applications. Firstly, in view of shortening development cycles and reducing development costs, early stage assessment of the performances of different setups as well as various design parameters becomes very important [14][15]. Also, in reality, it is very difficult to study SNCR processes at large utility boilers directly through measurement because of the limited experimental access. Large space and strong turbulence cause a very poor accuracy and hinder the essential operational characteristics. Finally, improved computational design tools are needed for design and optimization of SNCR performance due to tightened emission regulations and requests for decreasing price of NOx emission controlling system [16]. By incorporating suitable mathematical representation of relevant physical phenomena taking place in SNCR system, CFD can give detailed insight into all flow variables and replace expensive and intrusive experimental tests [17][18][19].

Taking all of the above mentioned into account, the aim of this work is the incorporation of the reduced kinetic mechanism of deNOx processes taking place inside the SNCR facility. First step was testing of all relevant models preceding the incorporated mechanism on well-established experimental case of Kim [20]. Parametrization of urea thermolysis model was performed on one

case, yielding good agreement on all other cases. Furthermore, implemented mechanism was validated on the real industrial reactor for which experimental results can be found in the literature as well as on the case of municipal waste incinerator. Simulated results show satisfactory agreement of simulation results with measured data and encourage commercial application of developed framework.

2. MATHEMATICAL MODEL

In order to accurately represent all relevant physical phenomena occurring during the injection of urea-water solution (UWS) into hot flue gases mathematical description of processes is needed as follows:

- solution of gas phase;
- description of spray droplets motion inside the domain;
- evaporation of urea-water solution droplets;
- thermal decomposition of urea;
- chemical reactions taking place in the gas phase;
- accurate and computationally economical representation of turbulence.

Equations of continuum mechanics are based on the conservation laws for mass, momentum and energy. The general form of the time averaged conservation equation for any dependent variable φ of the continuous phase in the differential form is:

$$\frac{\partial}{\partial t}(\rho\varphi)+\frac{\partial}{\partial x_j}(\rho\varphi u_j)=\frac{\partial}{\partial x_j}(\Gamma_\varphi\frac{\partial\varphi}{\partial x_j})+S_\varphi, \tag{1}$$

where ρ is the density, u_j Cartesian velocity, Γ_φ diffusion coefficient, and S_φ is the source term of the dependent variable φ. The source term S_φ is used for the coupling of the liquid phase of spray droplets to the gaseous phase.

Experimental observations as well as the knowledge obtained from the instability analyses form the basis for numerical modelling of liquid spray. The most commonly used method for spray

calculation today is Discrete Droplet Method (DDM) [21] although in come special cases, such as dense spray regions near the nozzle, Euler–Eulerian multiphase approach is gaining increasing popularity [22]. Taking into account current state of CFD techniques, it would be practically impossible to solve differential equations for the trajectory, momentum, heat and mass transfer of every single spray droplet. DDM simplifies spray modelling by introducing parcels which are groups of identical non-interacting droplets. Thus, one member of the group, i.e. droplet of certain size, represents the behaviour of the complete parcel. That way, only differential equations of parcels are numerically solved which significantly reduces computation time and required computing power.

Droplet parcels are introduced in the flow domain with initial conditions of position, size, velocity, temperature and number of particles inside the parcel. Lagrangian description of motion is then used for tracking the parcels through the computational grid. A drawback of the standard DDM is the treatment of Lagrangian parcels as point sources for physical quantities for the Eulerian gas flow field.

From the Newton's second law of motion which states that the net force on an object is equal to the rate of change of its linear momentum in an inertial reference frame follows droplet momentum equation:

$$m_d \frac{du_{id}}{dt} = F_{idr} + F_{ig} + F_{ip} + F_{ib} \tag{2}$$

where md and u_{id} are droplet mass and droplet velocity respectively, F_{idr} is the drag force, F_{ig} is a force including the effects of gravity and buoyancy, F_{ip} is the pressure force and F_{ib} summarizes other external forces. Comparing the magnitude of all forces, the drag force is only relevant force for fuel spray injection application. Therefore follows:

$$m_d \frac{du_{id}}{dt} = F_{idr} \tag{3}$$

After integrating above equation, u_{id} could be obtained and from this we can solve differential equation for the trajectory:

$$\frac{dx_{id}}{dt} = u_{id} \tag{4}$$

In commercial CFD code AVL FIRE® turbulent dispersion, evaporation of droplets, the droplet-gas momentum exchange, secondary break-up, droplet collision and droplet-wall interaction are covered with set of models that are summarized in [23].

Droplet evaporation can be described by different methods in the rising level of complexity, such as: constant droplet temperature model, infinite diffusion model, effective diffusion model, vortex model and Navier-Stokes solution. For the purpose of this research Abramzon/Sirignano evaporation model was used to perform calculations [24]. This model represents the extension of classical droplet vaporization model [25] and includes important effects such as variable physical properties, non-unitary Lewis number in the gas phase and influence of Stefan flow on the heat and mass transfer. It requires a relatively small amount of computational time per droplet and therefore is convenient for spray calculations. Its suitability will be demonstrated in the proceeding section.

Despite numerous experimental studies [26][27][28] theoretical understanding of evaporation and decomposition of UWS droplets is still far from satisfactory. Although droplet evaporation can be described by different methods in the rising level of complexity, such as: constant droplet temperature model, infinite diffusion model, effective diffusion model, vortex model and Navier-Stokes equations solution, for the SNCR application theoretical study conducted by Birkhold et al. [29] is implemented in AVL FIRE® and represents optimum between results accuracy and computational demands. At elevated temperatures the evaporation of liquid starts. Since water has a boiling point below starting temperature of urea thermolysis, the gaseous species first

consist mainly of water. Whether is urea vapour also produced is questionable, since urea is known to decompose directly via thermolysis from solid or liquid. Birkhold's approach assumes two stage process – pure water evaporation until the droplet is composed of urea only and subsequent thermolysis. It is assumed that droplets remain spherical throughout the evaporation and decomposition processes, as well as that no crystallization of urea occurs between 373 and 406 K.

In order to evaluate the influence of solved urea on the evaporation of water, Rapid Mixing model is employed. Within this model infinite high transport coefficients are assumed for the liquid phase, resulting in spatial uniform temperature, concentration and fluid properties in the droplet, but those quantities will change in time [24]. The variation of urea concentration of the droplet can be evaluated by:

$$\frac{dY_u}{dt} = -\frac{\dot{m}_{vap}}{m_d} Y_u \qquad (5)$$

It should be noted that mass flow from liquid to gaseous phase is defined to be negative.

Urea melts at 406 K and the thermal decomposition of urea into ammonia and isocyanic acid starts. It is generally accepted that two different ways for the thermal decomposition can be derived:

- evaporation of molten/solid urea to gaseous urea, which decomposes in gas phase into NH_3 and HNCO;
- direct thermolysis from molten/solid urea to gaseous NH_3 and HNCO.

This model assumes the latter option and since there is no phase change of urea, an alternative way as used for the evaporation of water must be taken to calculate the urea decomposition rate. For this purpose Arrhenius-type expression is used:

$$\frac{dm_u}{dt} = -\pi D_d A e^{(-E_a/RT_d)} \qquad (6)$$

where A is a frequency rate and E_a is activation energy. Experimental data from Yim et al. [30] were used for a default parameter fit.

Coupling all of the above mentioned physical phenomena with the fully detailed chemistry is not advisable from the standpoint of both CPU time and memory. Therefore, CFD modelling with reduced kinetic models is widely adopted. In this study well established seven-step global kinetic mechanism for SNCR chemistry [13][12][31] from Brouwer [32] with optimized kinetics parameters [11] was embedded into existing numerical framework. The seven chemical reactions shown in Table 1 are used to predict the concentration of NO, NH_3 and HNCO.

Table 1. Seven step reaction mechanism

Reaction	Pre-exponential factor [cm/(mol s K)]	Exponent [-]	Activation energy [kcal/mol]
NH3+NO→N2+H2O+H	2.13E+01	5.3	58 039
NH3+O2→NO+H2O+H	8.83E+03	7.65	139 964
HNCO→H+NCO	1.39E+13	0.85	82 457
NCO+NO→N2O+CO	2.26E+15	0.0	- 6 214
NCO+OH→NO+CO+H	3.68E+09	0.0	0.0
N2O+OH→N2+O2+H	8.6E+04	0.0	20 005
N2O→N2+O	8.5 E+07	0.0	81 023

The most favoured method for modelling turbulent flows in industrial applications is the Reynolds Averaged Navier Stokes equations (RANS) with an appropriate turbulence model. Many turbulent models employ the concept of a turbulent viscosity or a turbulent diffusivity to

approximate the turbulent Reynolds stresses and the turbulent heat fluxes. Turbulence was modelled by the standard k-ε model. This is the most widely used turbulence model in CFD simulations of practical engineering applications. It is numerically robust, offering a reasonable compromise between computational effort and accuracy, and it is generally accepted that the k-ε model yields reasonably realistic predictions of major mean-flow features in most situations [33]. For these reasons, the k-ε model is used in this work.

3. KIM CASE

3.1. Settings

Kim measured urea solution evaporation in hot exhaust gas to get values for NH_3 conversion rates [20]. Figure 1 shows scheme of experimental section with locations of sampling probes. Different distances from nozzle locations corresponding to different residence time are used to calculate NH_3 conversion efficiency when quasi-steady state is reached.

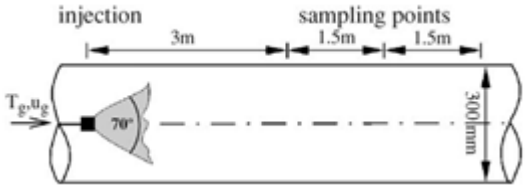

Figure 1. Schematic view of the experimental section from Kim [20]

In the commercial CFD code used, an evaporation model for spray can be tuned with two parameters. The parameters E4 – activation energy and E5 frequency factor are steering thermolysis model for the droplet mass transfer with respect to NH_3 conversion rate. Figure 2 shows computational domain consisting of 65 452 hexahedral elements.

At the outlet of the domain, the pressure boundary condition was imposed, whilst the domain wall was described with adiabatic boundary condition. Inlet air temperature and normal velocities were varied according to the table below, giving in total nine simulation cases. Assumed turbulence quantities on the inlet were 0.001 m2/s2 for turbulent kinetic energy and

0.03 m for turbulent length scale. For the simulation the standard k-ε turbulence model was used. Aqueous urea solution was directly injected inside the duct through the six holes of nozzle exit with particle size distribution approximated by Rosin-Rammler distribution whose parameters were experimentally determined in [20].

Table 2. Inlet condition variations

Case	**Gas Temperature**	**Average velocity**
	[°C]	[m/s]
1	300	6.55
2	300	9.04
3	300	10.99
4	350	6.39
5	350	9.08
6	350	10.77
7	400	6.03
8	400	8.33
9	400	10.84

For the turbulence and energy transport equations a first order UPWIND differencing scheme was applied, whilst for the continuity equation the central differencing scheme (CDS) was employed. Finally, for the momentum equation a combination of CDS and UPWIND was proposed by introducing the blending factor of 0.5 [23]. For all calculations the implicit time integration was employed ensuring unconditional solution stability, whilst the accuracy was achieved by employing sufficiently small time step of 1e-03 s. The solution convergence criterion is achieved when the momentum, pressure and energy residuals decrease under the

value of 1e-4, and when the value of turbulence kinetic energy and turbulence length scale decrease under the value of 1e-03. The pressure velocity coupling of the momentum and continuity equation was obtained using the SIMPLE algorithm.

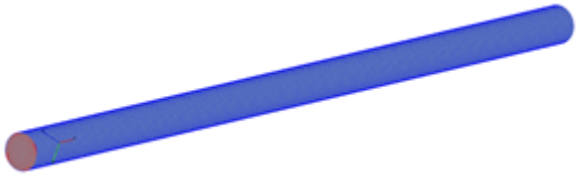

Figure 2. Kim case domain discretization

3.2.Results

On the following figures, comparison between the old parameters, new parameters and experimental measurements from Kim can be seen. New parameters show better agreement with experiment in all cases compared to the old ones. Both sets of parameters are shown in the Table 3.

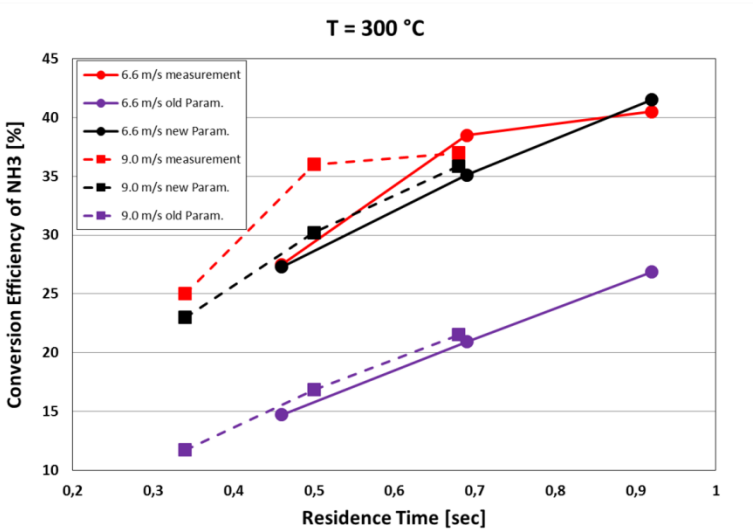

Figure 3. Comparison of results - Cases 1-3

Set of parameters, namely activation energy and frequency factor of Arrhenius equation, which was obtained by comparison of simulated results with experimental ones, yielded good agreement and was used for other cases in which exhaust gas mass flow and temperature were varied.

Table 3. Parameters of Arrhenius equation

	Activation energy, E4 J/mol	Frequency factor, E5 kg/(s m)
Old set	69 000	0.42
New set	66 376	0.57

In Figures 3, 4 and 5 it can be seen that the production of ammonia is increased as the temperature of the inlet air is increased. On the other hand, increase in the incoming gas velocities means the decrease of residence time and vice versa. Shortened residence time at the fixed temperature leads to the decrease in the amount of produced ammonia. Also, all results show the steep increases of ammonia production at entrance region and slow down further downstream.

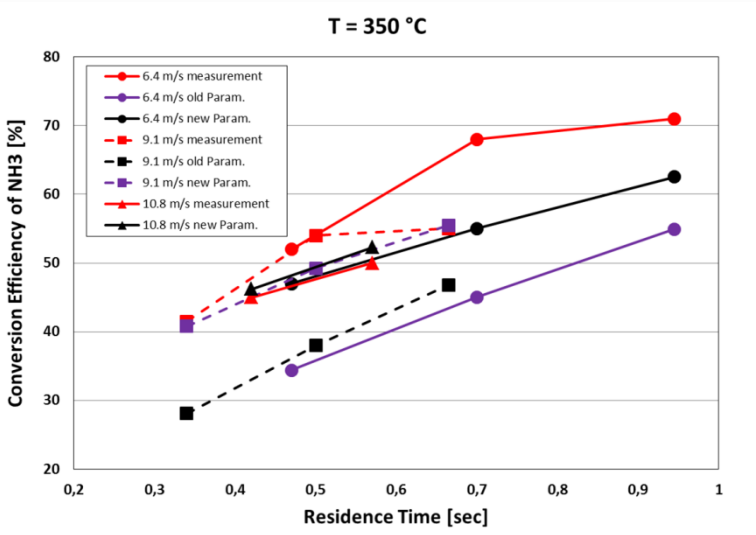

Figure 4. Comparison of results – Cases 4-6

Simulation of these cases predicted NH_3 conversion efficiency which satisfactory matches with measured data. It can be concluded that new parameter show good results in range of u = 9 m/s

of gas velocity. Also, performed simulations justify usage of Rapid Mixing model for droplet evaporation.

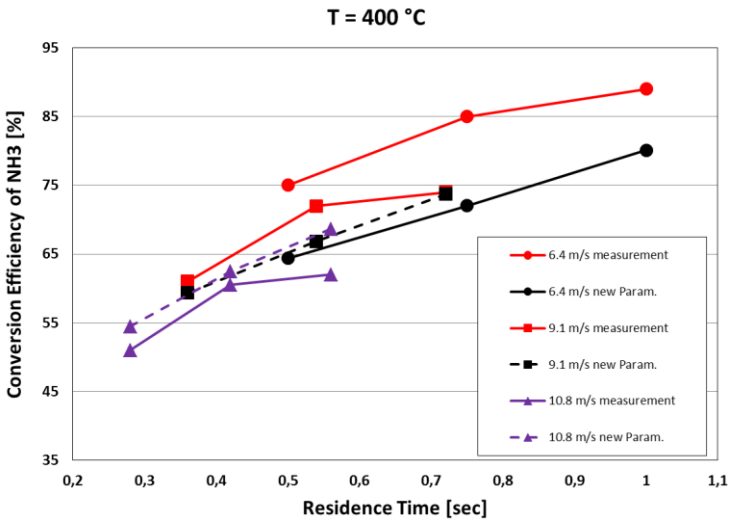

Figure 5. Comparison of results - Cases 7-9

4. NUMERICAL SIMULATION OF PIPE REACTOR

Figure 6 depicts the domain used in this research together with the boundary surfaces. In order to achieve mesh independency several computational meshes were examined. For the mesh dependency test, three meshes were generated consisting of 500 000, 200 000 and 107 000 control volumes, the last one being symmetrical. It has been observed that mean flow quantities inside the domain don't change significantly with decreasing mesh resolution to ≈ 200 000 control volumes. The same could be stated when employing symmetrical domain consisting of approximately 107 000 control volumes. Taking into account above stated, a symmetrical domain was selected for further research in order to maximize utilization of available computational resources. At the outlet of the domain, the pressure boundary condition was applied. The nozzle surface was defined with the constant temperature (1073 K) wall boundary condition.

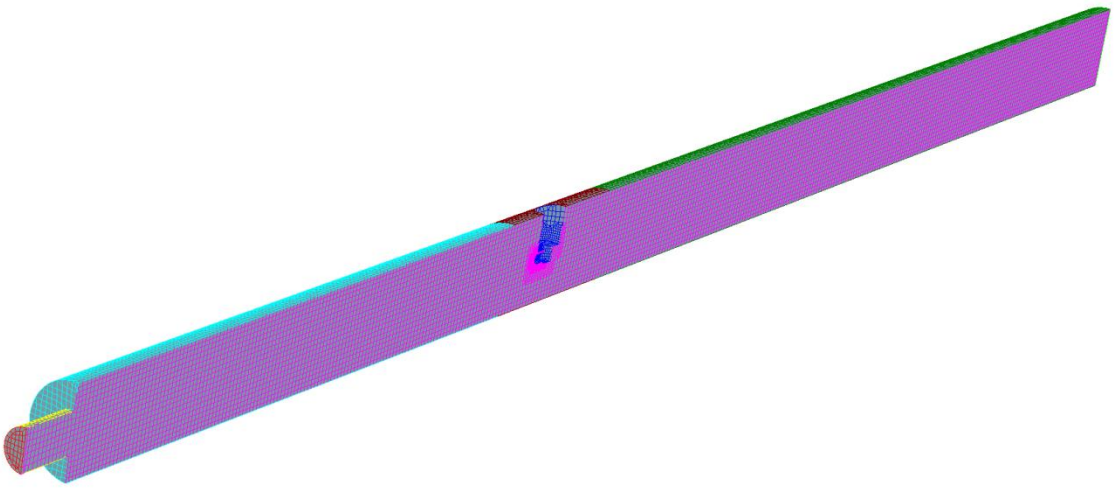

Figure 6. Computational domain with symmetric boundary condition

For the turbulence, momentum and energy transport equations a first order UPWIND differencing scheme was applied, whilst for the continuity equation the central differencing scheme (CDS) was employed. The CDS can generate numerical oscillations yielding unbounded and non-monotonic solutions. Therefore, for the momentum equation a combination of CDS and UPWIND was proposed by introducing the blending factor of 0.5 [23]. For all calculations the implicit time integration was employed ensuring unconditional solution stability, whilst the accuracy was achieved by employing sufficiently small time step of 1e-04 s. The solution convergence criterion is achieved when the momentum, pressure, energy and volume fraction residuals decrease under the value of 1e-4. The pressure velocity coupling of the momentum and continuity equation was obtained using the SIMPLE algorithm. Air entered the domain with prescribed constant mass flow through the inlet with diameter of 100 mm. Finally, turbulence quantities on the inlet were 10 % for turbulent intensity [11] and turbulent length scale was assumed to be 0.007 m. Urea water solution was injected into domain with particle size distribution approximated by Rosin-Rammler distribution with mean droplet diameter of 36 μ m and spreading parameter value of 3 [11]. Other details can be found in experimental investigations performed in [11]. Influence of the temperature on the SNCR

process efficiency was performed through the simulation of three experimental cases with various inlet temperature, as shown in the Table 4.

Table 4. Simulated cases

Case name	Inlet gas temperature, K
Case 1	1325
Case 2	1348
Case 3	1365

4.1 Results

This section presents results of on the previously described real industrial case of pipe reactor.

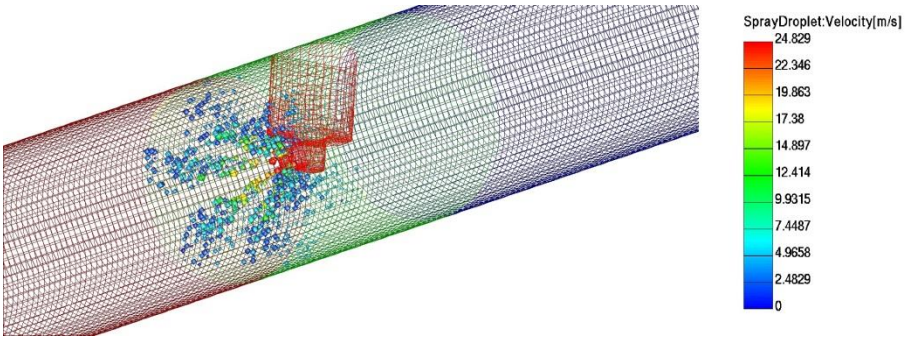

Figure 7. Spray injection

Figure 7 depicts the injection of urea water solution in the experimental pipe. Furthermore, here the droplet diameter and velocities are given. Blue particles represent slower droplets, and red particles represent faster particles, respectively. The droplets lose their mass due to the evaporation of water and urea thermolysis. Six injection spray cones can also be observed.

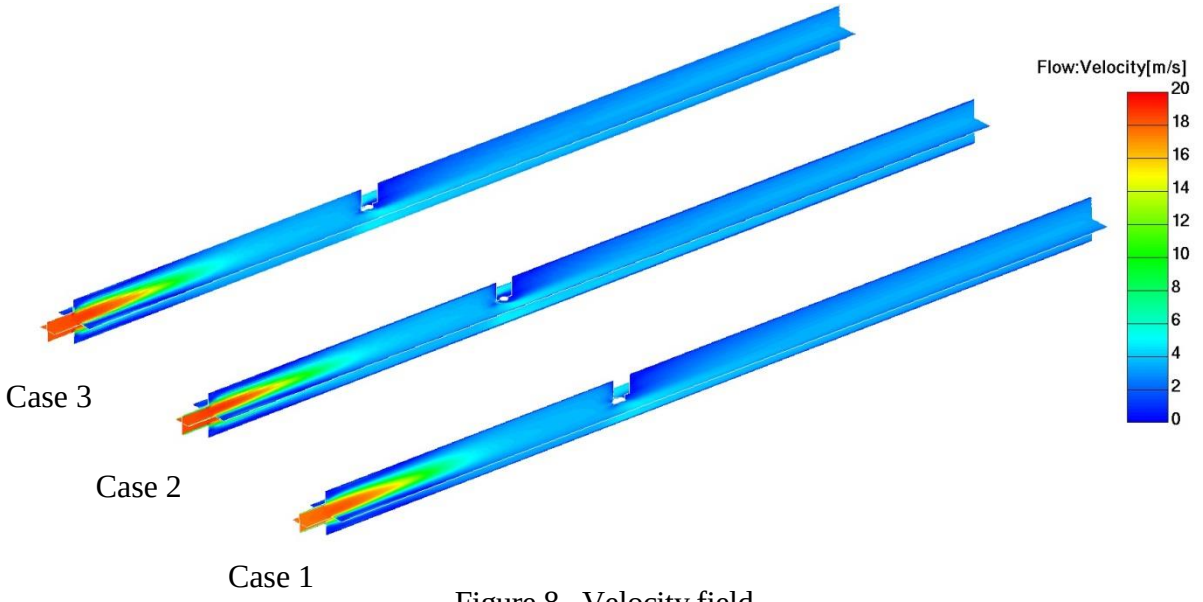

Figure 8. Velocity field

In the Figure 8 the velocity field inside the calculated experimental pipe is given for all simulated cases. As can be expected, velocity field of all cases is identical, since only inlet temperature was varied. On the left hand side of the figure, where the inlet is positioned, velocity is the highest. As the flow gets closer to the injector, it slows down, and afterwards has a stable profile with the velocity of around 5 m/s giving residence time for a reagent of about 0.3 s.

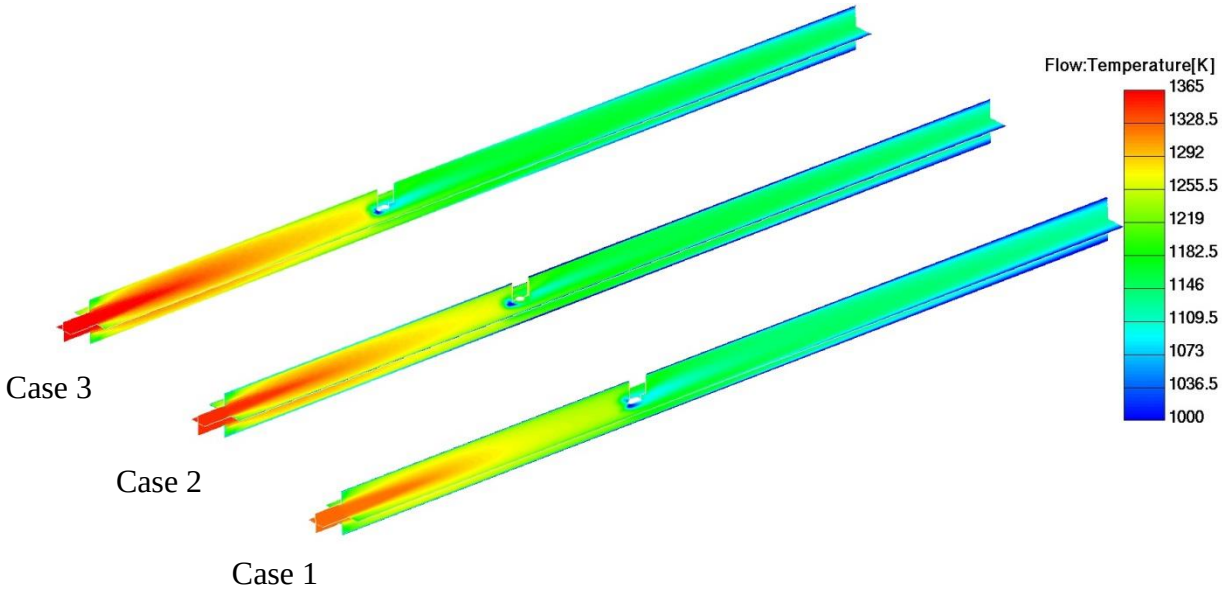

Figure 9. Temperature field

In Figure 9 the temperature field inside the calculated experimental pipe is given. Also, on the left hand side of the figure, where the inlet is positioned, the highest temperature can be observed. In the first part of the experimental pipe, the flow cools down only due to heat transfer to cooler walls. Linear temperature drop along pipe length has been assumed which correlates well with experimental measurements [11]. As the flow gets closer to the injector, the temperature decreases significantly due to the water evaporation and thermolysis of urea, and afterwards has a stable value between 1100 and 1200 K, depending on the simulated case. Temperature is vital factor affecting deNOx efficiency and in the following, the influence of temperature field on the concentration of different species is shown.

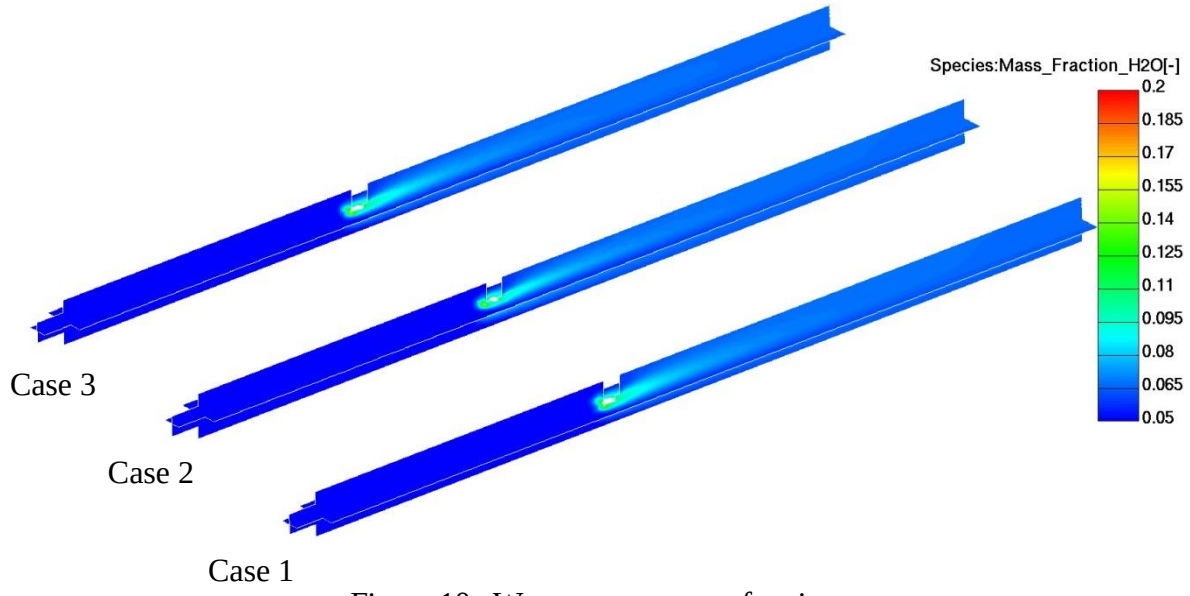

Figure 10. Water vapour mass fraction

In Fig. 10 the water vapour concentration inside the calculated experimental pipe is given. High temperature difference between the flow and injected urea water solution causes almost instantaneous evaporation of water content from droplets, which consequently means that the highest water concentration is in the vicinity of injector. After the injector, concentration stabilizes at the average value of around 8 % and there is no significant difference between three simulated cases. It is a reasonable result which shows that temperature difference

between flow and UWS solution is so high that temperature variation in simulated cases doesn't affect rapid water evaporation.

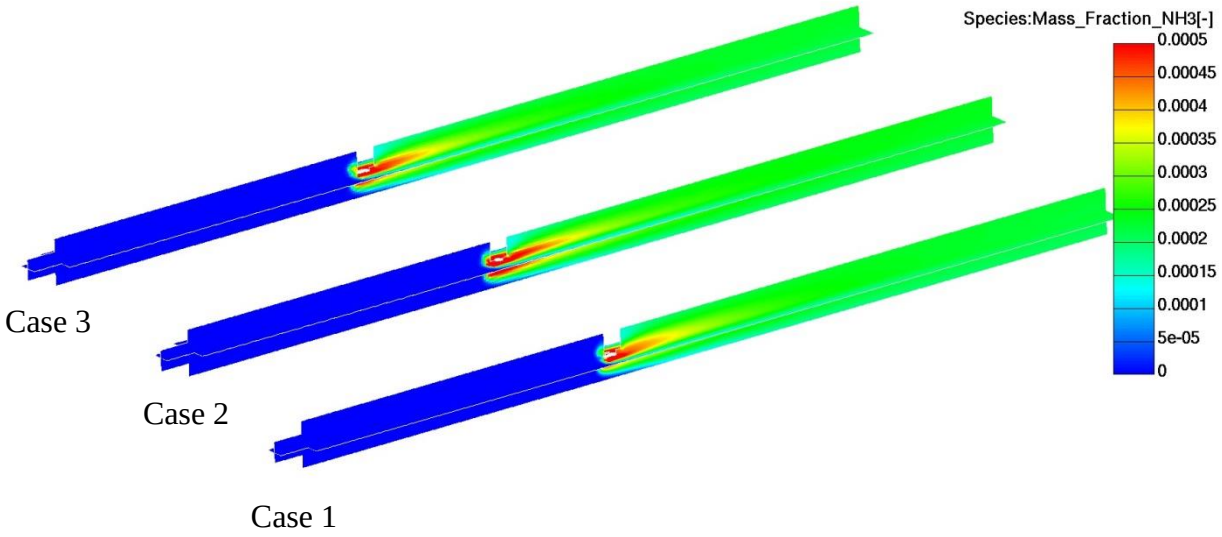

Figure 11. Ammonia mass fraction

Thermolysis of urea is taking place after water content of droplets gets below 5 %. Urea is decomposed in equimolar amounts to ammonia and isocyanic acid. Comparison of Figures 11 and 12 reveals that isocyanic acid is consumed in reactions with NO much more than NH3, indicating favourable simulation temperatures for former reactions. Comparison of simulated cases reveals that conditions in the first case yield the most favourable results in terms of production of a HNCO.

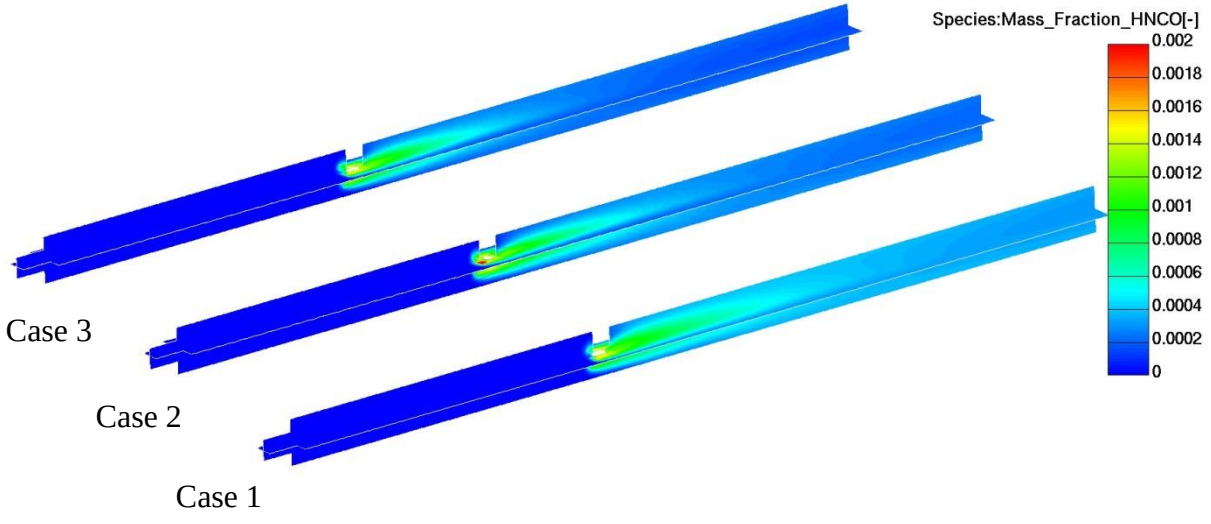

Figure 12. Iscocyanic acid mass fraction

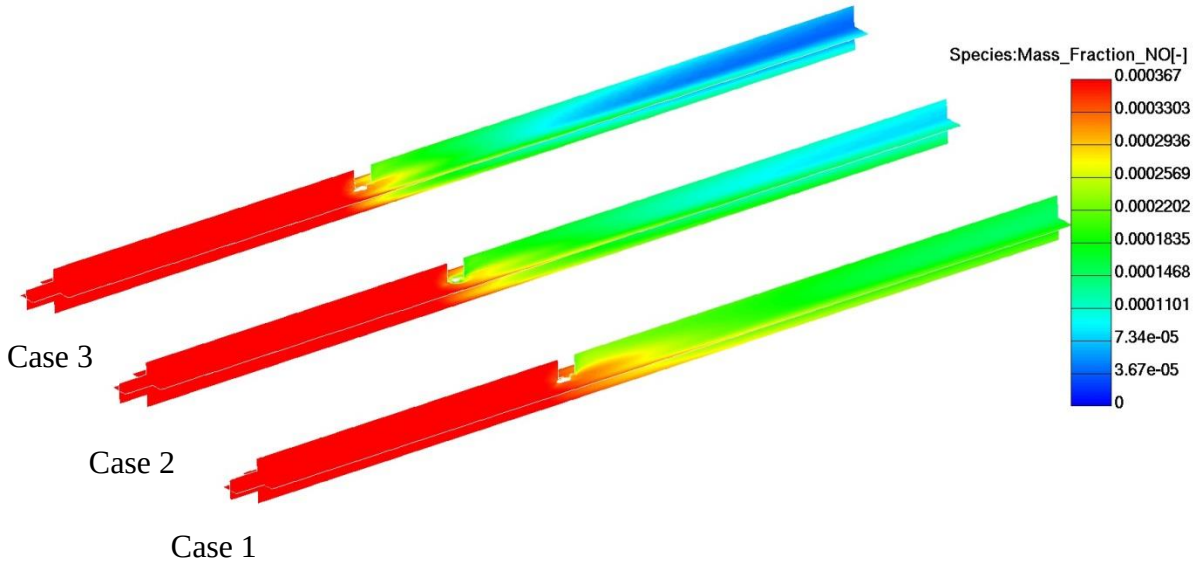

Figure 13. NO mass fraction

Figure 13 shows NO concentration reduction inside the calculated experimental pipe which is the final aim of SNCR process. As the inlet flow temperature of simulated cases increases, NO reduction also increases. Connection with the consumption of HNCO is clearly visible, where third case with highest HNCO consumption yields the best NO reduction. In the injector region, due to the reaction of HNCO with NO, the NO mass fraction starts to decrease and continues so by flowing further downstream, which is equivalent to increase in reaction residence time.

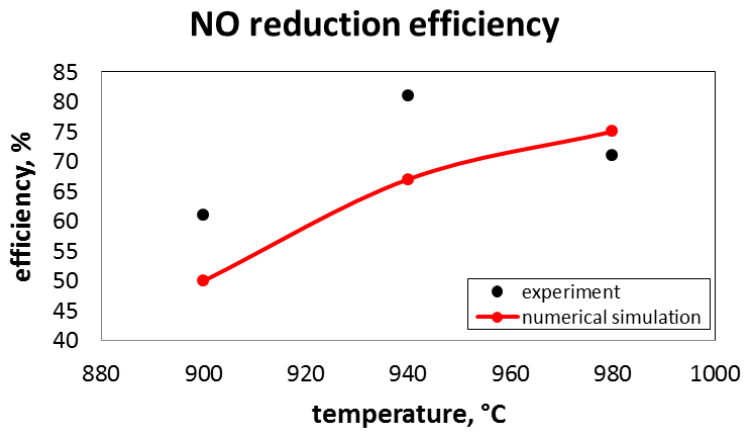

Figure 14. Comparison of experimental and numerical results

Finally, in Figure 14 the comparison of experimental measurements with numerical predictions is given. The results are compared at the location of the measurement probe 200 mm before the pipe exit. Here it should be noted that the mean value for the numerical results was taken, since the location of the probe within the experimental pipe cross section is not mentioned. The numerical predictions show satisfying agreement with the experimental ones, although trend seen in experiment is not captured by the simulation. Contrary to simulations where NO reduction efficiency rises steadily with increasing temperature, experimental data show maximum in second case and then NO reduction efficiency drops afterwards. The reason behind this discrepancy may lay in the fact that linear temperature drop of the wall fitted from experimental measurements was provided only for the third case, which consequently shows the best agreement with NO reduction measurement. For cases 1 and 2 authors made an approximation on the inlet air temperature based on physical reasoning, but it can be clearly seen that some crucial information from experiment are needed for more accurate simulation. However, satisfactory agreement with experimental results gives reasonable confidence for industrial application of described model, described in the following section.

5. NUMERICAL SIMULATION OF INDUSTRIAL INCINERATOR

Simple test cases are appropriate for checking the quality of individual implemented models or few of them, but the synergy of all physical models describing certain industrial application should be validated on some real industrial case for which, ideally there are some confident experimental measurements. Figure 15 depicts computational domain used in research of industrial incinerator together with the boundary surfaces. In order to achieve mesh independency several computational meshes were examined. After evaluation, a computational domain consisting of 179 106 control volumes was selected. The most of those volumes were created in hexahedronal shape, especially in the regions of the utmost interest, such as injection point of the urea-water solution. To fully account the turbulent flow within

the system a 3D computational mesh was used. The full detail on the geometry of the system can be found in [13].

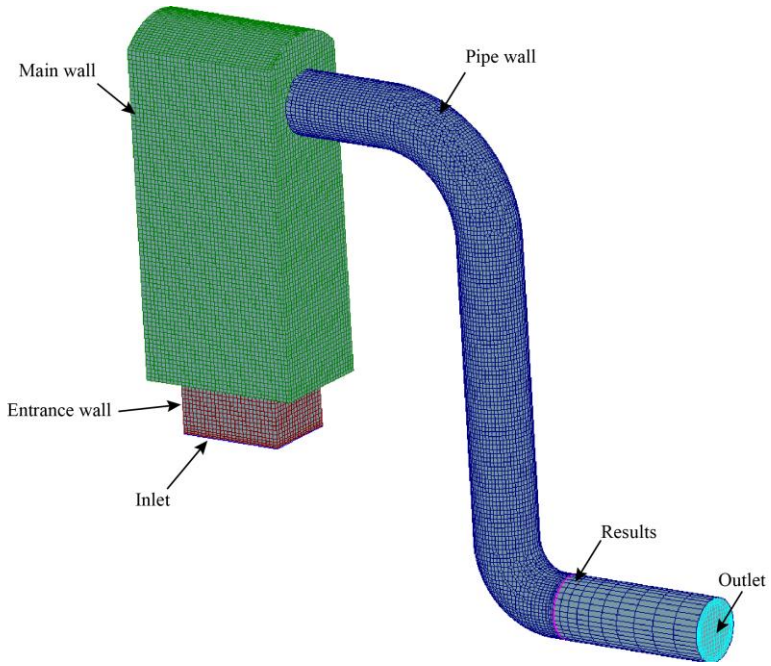

Figure 15. Computational domain of the incinerator

At the inlet a mixture of gases (NO, CO2, O2, N2) with the temperature of 830°C and a mass flow rate of 4.6602 kg/s enters the domain. The normal velocity taken from the experiments is 6 m/s. The temperature of the incinerator wall decreases as a result of heat loss to the surrounding. The temperature on the entrance wall reduces for 30 °C/m, on the main wall for 15 °C/m, whilst the pipe wall temperature is held at the constant temperature of 660 °C. The results were recorded at the Results selection. The location of this selection corresponds to the location of the measured data. The domain was prolonged from the selection Results to the Outlet selection to achieve the parabolic boundary conditions. At the outlet of the domain, the pressure boundary condition was applied. The 4 % urea-water solution is injected into the domain using three injectors with constant velocity of 25 m/s. The droplet disintegration models were replaced by presuming the droplet size distribution. The mean droplet diameter

of the solution was 45 microns for the observed nozzle system. It is of utmost importance to correctly describe the spray process since the evaporation rate and the mixing between the droplet phase and bulk phase directly influence the thermolysis process and NO reduction. The Rosin–Rammler distribution with spread parameter value of 3 was used to represent the non-uniform droplet size distribution [13]. The urea-water solution spray at the developed state is shown in Figure 16.

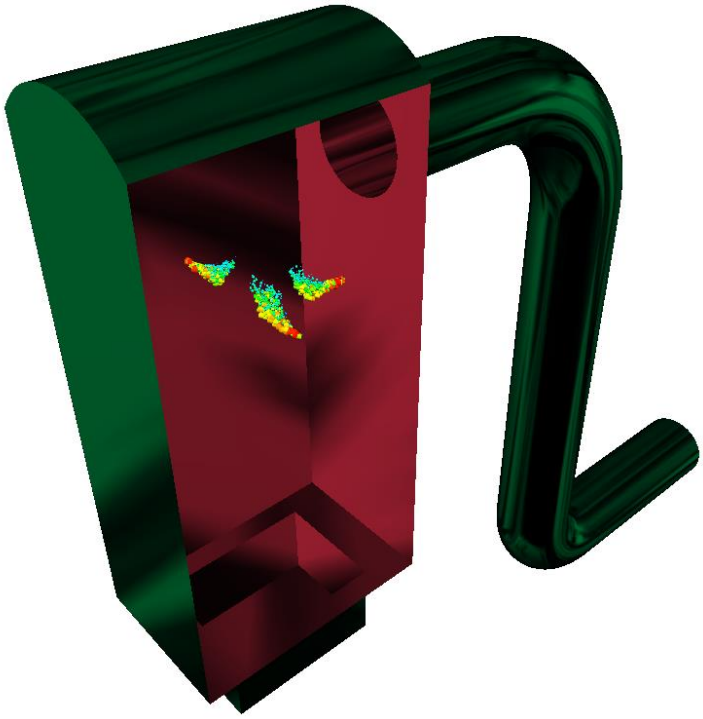

Figure 16. Urea-water solution spray at the developed state

The same reduced kinetic model from Brouwer depicted in the Table 1 was employed to describe the chemistry processes occurring in the system. The NO reduction was achieved with reaction of the nitrogen oxide with the species generated from the thermolisys of the urea-water solution.

The numerical setup of the simulation was taken the same as in the previously validated numerical simulation of pipe reactor. The time step was set to 1e-04 s and it was conditioned with the used reaction mechanism. Simulation used turbulence settings as follows: 8% turbulence intensity on the inlet and hydraulic diameter of 1.627 m [13]. With the given time

discretisation and numerical setup, the simulation was stable and convergence of the solution in each time step was achieved.

5.1.Results

In Figure 17 several quantities of interest are shown for the initial stage (0.5 s) of urea injection and for the quasi-stationary state reached at 10 s. The first column shows the temperature field for mentioned time frame. Initially the gas mixture starts to flow into the incinerator with 6 m/s velocity and temperature of 1273.15 K. For better convergence and for reducing the simulation time the whole domain was initialised with the conditions that occur at the inlet selection. Therefore, in the whole domain at the initial state the NO was present in a certain amount. The urea-water solution was injected into the domain via three nozzles with total injected mass of 0.0107 kg/sec. The endothermal thermolysis process occurred in the region where the urea-water solution droplets are injected, as visible on the first column in Figure 17. Therefore, the temperature reduction can be addressed to the thermolysis of the injected solution. The thermolysis process is modelled according to the model described in the previous section. The second column shows the results of the 0D reactor model used for calculation of species reaction rates according to the seven step chemical mechanism. The NO reduction rate is visible and in accordance with the used mechanism. The negative NO reduction rate, that is visible in the second column, influences the overall NO species mass concentration. The spatial NO concentration is shown in the last column of Figure 17 and the border between zone of high NO concentration and zone with reduced concentration is actually the curve that correspond well to the NO reduction rate. However, due to the current nozzle positioning a certain amount of gas mixture containing high NO concentration passes into the pipe and outflows together with gas mixture with removed NO species.

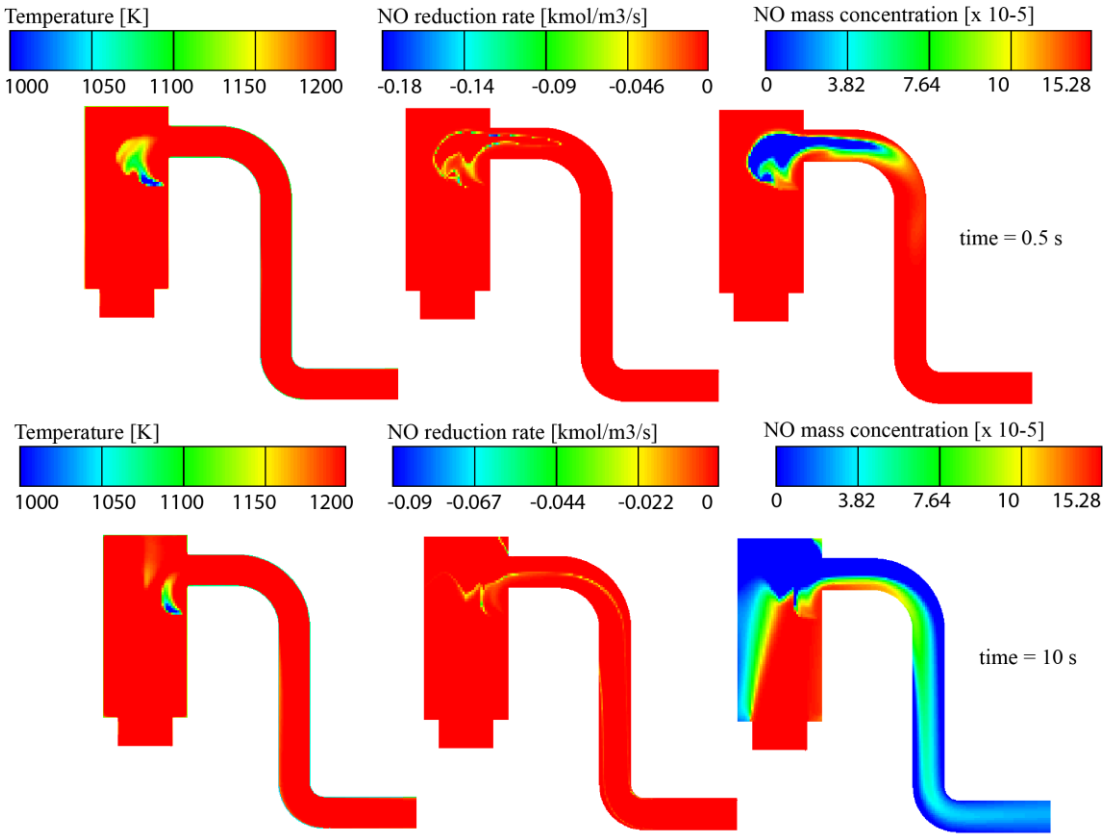

Figure 17. Flow temperature, NO reduction rate and NO mass concentration for two time points

Figure 18 shows the velocity field together with water and ammonia mass fraction for two different time instances. The average velocity value, after quasi steady state has been reached, is approximately 6 m/s inside the incinerator and increases to 10 m/s in the exit pipe due to the continuity law. It would be expected that increased velocity will cause better reagent mixing in the exit pipe. However, as can be seen in the last column of the Figure 18, this is not the case, since most of the ammonia is consumed in the SNCR process before even reaching the exit pipe. The injected water from UWS evaporates completely before the exit pipe and is diluted to minuscule quantities by turbulent mixing.

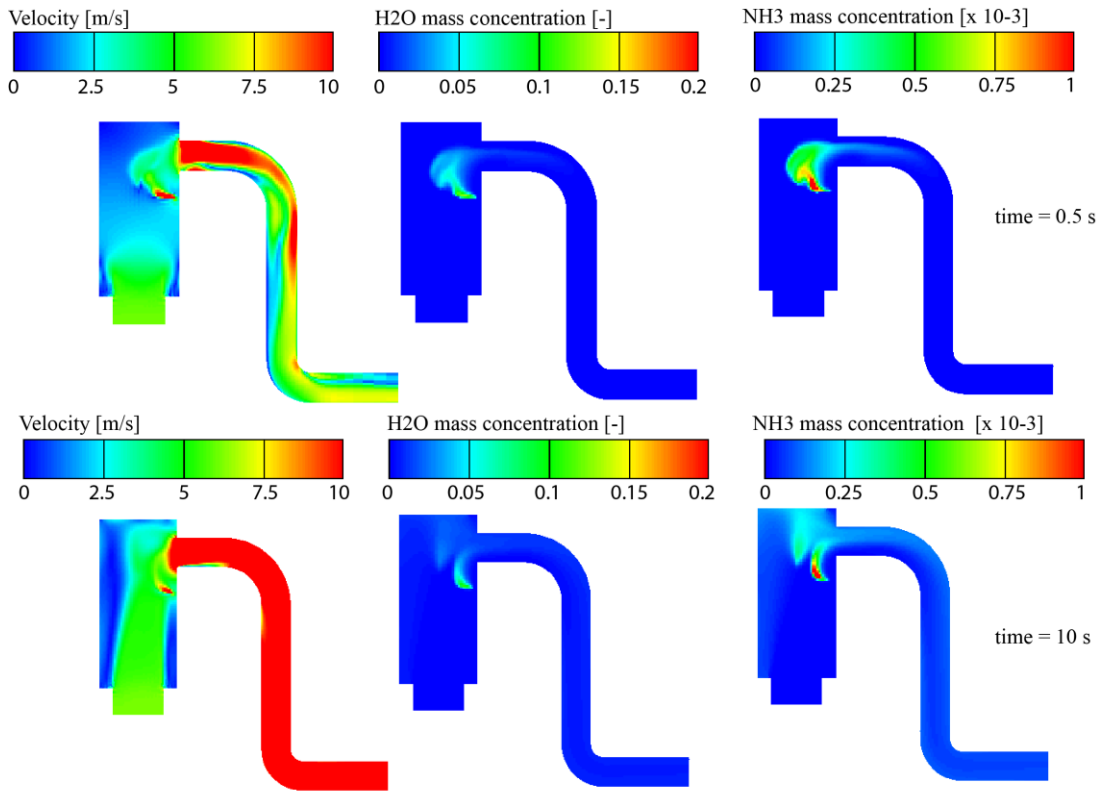

Figure 18. Flow velocity, H_2O and NH_3 mass fraction for two time points

The mix of reduced and the NO rich zone passes through selection at the outflow of the pipe, as shown in Figure 19. This position corresponds to the measurement position from the experiment which is used to calculate the NO reduction. In experimental research the recorded NO outlet concentration was 45 ppm whilst in the simulation was 22.5 ppm. On the first sight it may look as a big discrepancy, but one should take into account that object is a miniscule quantity and also the position of the measurement probe was not indicated within the reference paper. Comparison with the outlet temperature is excellent with only 0.2 % discrepancy (932°C compared to measured temperature of 930°C). This implies that the numerical setup is correctly chosen and the used models are well implemented. Also, it means that the initial and boundary conditions are defined in correct way and are in a good agreement with the experimental setup. Finally, it has been proven that developed model can be used as a part of development process of real industrial facilities.

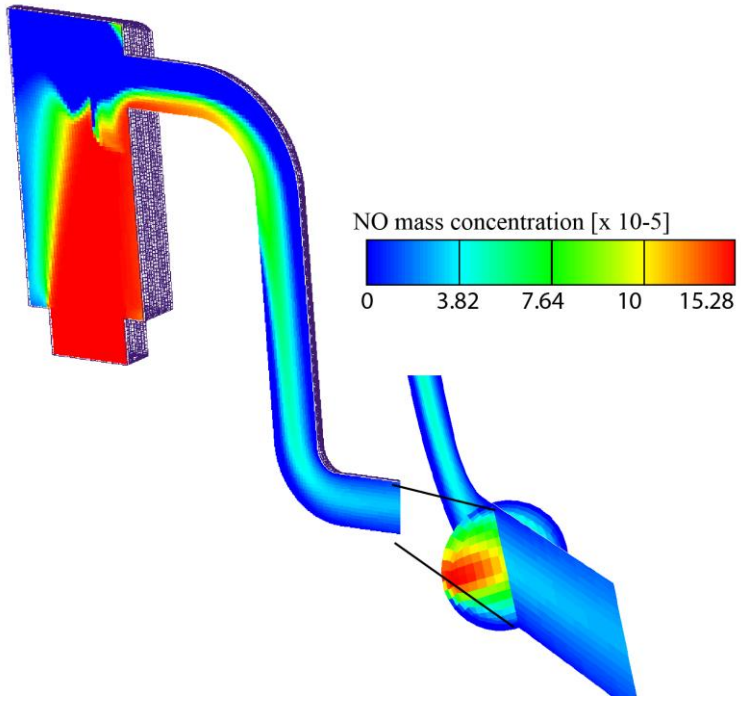

Figure 19. The NO mass fraction reduction from the inlet to the point of experimental measurement

6. CONCLUSION

This paper presented CFD modelling capabilities of physical phenomena taking place in the SNCR process. After the literature review, existing numerical framework was extended by incorporation of the suitable seven step reaction mechanism from Brouwer. It has been proven as sufficiently accurate and not too demanding from computational point of view.

First step was validation and parametrization of urea decomposition model on the case of Kim. Parametrization obtained on one of the test cases proved as satisfactory accurate also on all other cases. Afterwards, a 3D turbulent reacting flow CFD model involving reaction mechanism was applied on the experimental case which closely resembles real SNCR application. Results of the conducted numerical study show satisfactory agreement with measured data in terms of NO reduction efficiency but the experimental trend was not captured by simulations. Finally, the set numerical framework was applied in the simulation of the large scale incinerator SNCR process,

for which measurement data exist. The results show that the numerical prediction of the NO reduction is in the line with the measured NO reduction. Summarizing the results of this study, it can be concluded that the developed model may be a valuable contribution in continuous process where constant improvement of accuracy of the physical models used in CFD is mandatory in order to comply with the ever increasing requirements of the industry and emission regulations.

ACKNOWLEDGMENTS

Financial support from the European Union's seventh Programme managed by REA - Research Executive Agency (FP7/2007-2013) under Grant agreement PIRSES-GA-2011-294933 (DISKNET project) is gratefully acknowledged.

REFERENCES

[1] Cause of climate change n.d. http://ec.europa.eu/clima/change/causes/index_en.htm (accessed July 28, 2015).

[2] European Environment Agency. Nitrogen oxides (NOx) emissions n.d. http://www.eea.europa.eu/data-and-maps/indicators/eea-32-nitrogen-oxides-nox-emissions-1/assessment.2010-08-19.0140149032-3 (accessed July 15, 2015).

[3] European Union, Regulation (EC) No 715/2007. 2007.

[4] Mahmoudi S, Baeyens J, Seville JPK. NOx formation and selective non-catalytic reduction (SNCR) in a fluidized bed combustor of biomass. Biomass and Bioenergy 2010;34:1393–409. doi:10.1016/j.biombioe.2010.04.013.

[5] Mehmood S, Reddy B, Rosen M. Emissions and Furnace Gas Temperature for Electricity Generation Via Co-Firing of Coal and Biomass. J Sustain Dev Energy, Water Environ Syst 2015;3:344–58. doi:10.13044/j.sdewes.2015.03.0026.

[6] Palash SM, Masjuki HH, Kalam MA, Masum BM, Sanjid A, Abedin MJ. State of the art of NOx mitigation technologies and their effect on the performance and emission characteristics of biodiesel-fueled Compression Ignition engines. Energy Convers Manag 2013;76:400–20. doi:10.1016/j.enconman.2013.07.059.

[7] Kozarac D, Vuilleumier D, Saxena S, Dibble RW. Analysis of benefits of using

internal exhaust gas recirculation in biogas-fueled HCCI engines. Energy Convers Manag 2014;87:1186–94. doi:10.1016/j.enconman.2014.04.085.

[8] European Union, Directive 2000/76/EU. 2000.

[9] European Union, Directive 2010/75/EU. 2010.

[10] Li Z, Liu XM, Yang DH, Qin WJ, Yang GS, Zhang DL. Research of the SNCR Process and its Application. Adv Mater Res 2014;953-954:1307–14. doi:10.4028/www.scientific.net/AMR.953-954.1307.

[11] Nguyen TDB, Lim Y Il, Kim SJ, Eom WH, Yoo KS. Experiment and computational fluid dynamics (CFD) simulation of urea-based selective noncatalytic reduction (SNCR) in a pilot-scale flow reactor. Energy and Fuels 2008;22:3864–76. doi:10.1021/ef8004652.

[12] Xia Z, Li J, Wu T, Chen C, Zhang X. CFD simulation of MSW combustion and SNCR in a commercial incinerator. Waste Manag 2014;34:1609–18. doi:10.1016/j.wasman.2014.04.015.

[13] Nguyen TDB, Kang T-H, Lim Y-I, Eom W-H, Kim S-J, Yoo K-S. Application of urea-based SNCR to a municipal incinerator: On-site test and CFD simulation. Chem Eng J 2009;152:36–43. doi:10.1016/j.cej.2009.03.025.

[14] Xu Y, Zhang Y, Wang J, Yuan J. Application of CFD in the optimal design of a SCR–DeNOx system for a 300MW coal-fired power plant. Comput Chem Eng 2013;49:50–60. doi:10.1016/j.compchemeng.2012.09.014.

[15] Mikulč ić H, Vujanović M, Fidaros DK, Priesching P, Minić I, Tatschl R, et al. The application of CFD modelling to support the reduction of CO2 emissions in cement industry. Energy 2012;45:464–73. doi:10.1016/j.energy.2012.04.030.

[16] Kapitler M, Samec N, Kokalj F. Numerical optimization of a waste-to-energy plant's operating parameters using CFD. Therm Sci 2011;15:1–16. doi:10.2298/TSCI101004084K.

[17] Samec N, Kokalj F, Chen J-Y. Combustion Simulation in the Secondary Chamber of a Pilot-Scale Incinerator. Environ Eng Sci 2007;24:905–16. doi:10.1089/ees.2006.0154.

[18] An H, Yang WM, Li J, Zhou DZ. Modeling analysis of urea direct injection on the NOx emission reduction of biodiesel fueled diesel engines. Energy Convers Manag 2015;101:442–9. doi:10.1016/j.enconman.2015.06.008.

[19] Honus S, Juchelková D. Mathematical models of combustion , convection and heat transfer in experimental thermic device and verification. Tech Gaz 2014;21:115–22.

[20] Kim JY, Ryu SH, Ha JS. Numerical Prediction on the Characteristics of Spray-Induced Mixing and Thermal Decomposition of Urea Solution in SCR System. ASME 2004 Intern. Combust. Engine Div. Fall Tech. Conf., ASME; 2004, p. 165–70. doi:10.1115/ICEF2004-0889.

[21] YUEN MC, CHEN LW. On Drag of Evaporating Liquid Droplets. Combust Sci Technol 1976;14:147–54. doi:10.1080/00102207608547524.

[22] Vujanović M, Petranović Z, Edelbauer W, Baleta J, Duić N. Numerical modelling of diesel spray using the Eulerian multiphase approach. Energy Convers Manag 2015;104:160–9. doi:10.1016/j.enconman.2015.03.040.

[23] AVL. FIRE ® VERSION 2013.2 manual. 2013.

[24] Abramzon B, Sirignano WA. Droplet vaporization model for spray combustion calculations. Int J Heat Mass Transf 1989;32:1605–18. doi:10.1016/0017-9310(89)90043-4.

[25] Dukowicz JK. Quasi-steady droplet phase change in the presence of convection. 1979.

[26] S. Kontin, A. Höfler, R. Koch H-JB. Heat and Mass Transfer accompanied by Crystallisation of single Particles containing Urea-water-solution. Proc. 23rd ILASS-2010, Brno: ILASS; 2010.

[27] Musa, S. N. A., Saito, M., Furuhata, T., Arai M. Evaporation characteristics of a single aqueous ureasolution droplet. ICLASS 2006, 2006.

[28] Wang TJ, Baek SW, Lee SY, Kang DH, Yeo GK. Experimental investigation on evaporation of urea-water-solution droplet for SCR applications. AIChE J 2009;55:3267–76. doi:10.1002/aic.11939.

[29] Birkhold F, Meingast U, Wassermann P, Deutschmann O. Modeling and simulation of the injection of urea-water-solution for automotive SCR DeNOx-systems. Appl Catal B Environ 2007;70:119–27. doi:10.1016/j.apcatb.2005.12.035.

[30] Yim SD, Kim SJ, Baik JH, Nam IS, Mok YS, Lee JH, et al. Decomposition of urea into NH3 for the SCR process. Ind Eng Chem Res 2004;43:4856–63. doi:10.1021/ie034052j.

[31] Farcy B, Abou-Taouk A, Vervisch L, Domingo P, Perret N. Two approaches of chemistry downsizing for simulating selective non catalytic reduction DeNOx process. Fuel 2014;118:291–9. doi:10.1016/j.fuel.2013.10.070.

[32] Brouwer J, Heap MP, Pershing DW, Smith PJ. A model for prediction of selective noncatalytic reduction of nitrogen oxides by ammonia, urea, and cyanuric acid with mixing limitations in the presence of co. Symp Combust 1996;26:2117–24. doi:10.1016/S0082-0784(96)80036-1.

[33] Blazek J. Computational Fluid Dynamics: Principles and Applications. Amsterdam, London, New York, Oxford, Paris, Shannon, Tokyo: Elsevier; 2001.

Figure captions:

Figure 1. Schematic view of the experimental section from Kim [20]

Figure 2. Kim case domain discretization

Figure 3. Comparison of results - Cases 1-3

Figure 4. Comparison of results – Cases 4-6

Figure 5. Comparison of results - Cases 7-9

Figure 6. Computational domain with symmetric boundary condition

Figure 7. Spray injection

Figure 8. Velocity field

Figure 9. Temperature field

Figure 10. Water vapour mass fraction

Figure 11. Ammonia mass fraction

Figure 12. Iscocyanic acid mass fraction

Figure 13. NO mass fraction

Figure 14. Comparison of experimental and numerical results

Figure 15. Computational domain of the incinerator

Table captions: